Design of Wideband SPDT RF Switch Using Switchable DGS for Sustainable Wireless Systems

Adib Othman^{1*}, Noor Azwan Shairi¹, Huda A Majid², Faiz Asraf Saparudin², Zahriladha Zakaria¹, Najib Al-Fadhali³

¹Fakulti Teknologi dan Kejuruteraan Elektronik dan Komputer & Centre for Telecomunication Research & Innovation, Universiti Teknikal Malaysia Melaka, Hang Tuah Jaya, Durian Tunggal, Melaka, 76100, Malaysia

²Fakulti Teknologi Kejuruteraan, Universiti Tun Hussein Onn Malaysia, Hub Pendidikan Tinggi Pagoh, Muar, Johor, 84600, Malaysia

³Electrical Engineering Technology Alfred State College of Technology, State University of New York, 10 Upper College Drive Alfred, New York, 14802, USA

*adib@utem.edu.my

Abstract. This paper presents a single-pole double-throw (SPDT) switch that is integrated with a thin rectangular patch switchable defected ground structure (DGS). It is a novel technology for obtaining wideband and high isolation for the SPDT switch in millimeter-wave (mm-wave) telecommunications due to the usage of switchable DGS with bandstop and bandwidth enhancement capabilities. A wideband and high isolation are required for the switchable DGS SPDT switch to operate optimally in mm-wave frequency ranges, as well as to reduce the effect of leakage signal on both the transmitter and receiver connected to the SPDT switch and hence improve system efficiency and signal integrity. The SPDT switch design was combined with two small rectangular patches switchable DGSs that could switch between bandstop and allpass responses using biasing diodes on the DGS. As a result, the suggested SPDT switch with the switchable DGS had 6 dB of insertion loss and high isolation of more than 25 dB with wideband isolation of 25.24% fractional bandwidth, which was consistent with the simulation results. Furthermore, the isolation magnitude is doubled compared to the conventional SPDT switch. This work demonstrates that integrating switchable DGS into discrete SPDT switches provides a practical solution for realizing wideband, high-isolation performance suitable for 5G mm-wave where compactness and bidirectional reconfigurability is increasingly essential for sustainable RF front-end systems.

Keywords: Bandstop response, isolation, millimeter-wave, SPDT switch, switchable DGS, sustainable RF front-end system, wideband telecommunication.

(Received 2025-05-09, Revised 2025-09-10, Accepted 2025-10-18, Available Online by 2025-10-30)

1. **Introduction**

In general, radio frequency (RF) switches function by routing any RF signal in a transmission path to another path in two operating states: one with a very high impedance (open-circuit condition) and the other with a very low impedance (short-circuit condition). According to Shairi and Zobilah [1], RF switches are currently implemented in civilian systems and targeted for mass production. The most common applications of the RF switch in civilian systems are wireless communications for data exchange in various standards such as mobile telephone communication systems (currently 5G technology), wireless local area networks (WLAN), Wireless Fidelity (Wi-Fi), Wireless Sensing, Vehicle-to-everything (V2X), and Bluetooth and Millimeter Wave (mm-wave) technology.

An advantage of the mm-wave frequency spectrum is that it provides a wide bandwidth, which leads to higher peak data rates. Wide bandwidth and high data rates are the current demands in wireless communication to support the communication of many users in a dense population, such as 5G telecommunications, radar applications in V2X, and fast image processing in security sensing [2]. To date, the lower frequency spectrum is heavily used and most probably does not provide the desired wide bandwidths. Hence, the application of an RF front-end system in the mm-wave band is essential to meet the current needs.

To facilitate transmission (uplink transmission) and receive (downlink transmission) mode switching for Time Division Duplex (TDD) communication, RF switches, or more specifically discrete single-pole double-throw (SPDT) RF switches, are commonly employed in mm-wave frequency applications, as shown in Figure 1. This architecture has been suggested for use in 5G mm-wave communications, and 5G MIMO antennas must be coupled to SPDT switches [3]. To reduce any significant radio frequency (RF) power leakage from the transmitter to the receiver that can damage the active circuits of the receiver, particularly the low noise amplifier, high isolation between the transmitter and receiver is one of the crucial design factors for SPDT switches low noise amplifier (LNA).

Wideband isolation in the RF front-end system is essential for mm-wave wideband operation, as it caters to both uplink and downlink transmissions, which have specific frequency ranges for each operation. Because the system operates in wideband, wideband isolation allows for the integration of not only the RF transmitter and receiver on the same substrate, but also other devices in the RF front-end system, such as antennas. However, good isolation between the transmitter and receiver in the RF front-end system is a crucial consideration in the design of RF switches, particularly for high-power applications, such as base stations and wireless infrastructures [4]. Significant isolation is required to prevent high levels of RF power from leaking from the transmitter from the receiver through the off-state channel [5].

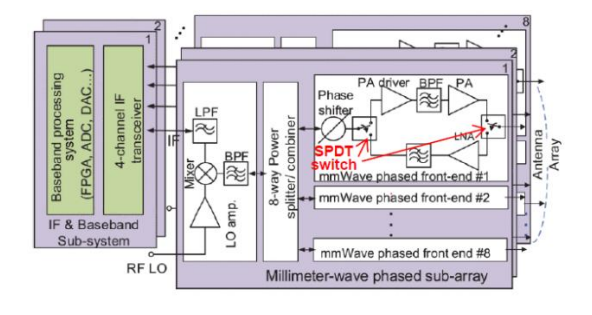


Figure 1. SPDT switch in a mm-wave transceiver architecture [3]

Meanwhile, research is being conducted on the application of a defected ground structure (DGS) in RF design for specific functions or parameter improvements. The guided wave characteristics of the microstrip line are modified by implementing a DGS, which changes the propagation constant; thus, the response is a bandstop filter [6], [7]. Therefore, the DGS has great potential, such as bandwidth enhancement, size compactness, and lowering insertion loss and return loss improvement [8], [9], [10]. Meanwhile, by implementing Positive-Intrinsic-Negative (PIN) diode on DGS, it has another

functionality where the resonance frequency of DGS can be switched between two responses: bandstop and allpass at a specific frequency range [11], [12]. Therefore, the DGS can be tuned to switchable DGS.

Even though the PIN diode used as a switching element in the discrete SPDT RF switch has its own isolation properties, it is still insufficient to provide high isolation owing to the parasitic reactance associated with the package leads, bond wires, and package material [13], [14]. Even though there are techniques such as multiple cascaded shunts or series and shunt combinations of PIN diodes to obtain high isolation in SPDT switches, as reported in [15], [16], [17], they produce a trade-off in increasing the size of the circuit owing to the quarter-wavelength spacing [18] between the PIN diodes and higher turn-on currents for the combination of PIN diodes.

Because the DGS has bandstop and bandwidth enhancement properties, its application in SPDT switches will result in wideband and high isolation with a minimized number of PIN diodes used, resulting in low heat generation and therefore improving the power handling capability of the switch. In addition, the recent RF front end system is dynamically bi-directional with either side of the SPDT switch can be transmitter or receiver [19], [20], usage of the DGS to produce wideband isolation is an advantage as the switchable DGS can be reconfigured to different responses with the help of biased PIN diode. Aftermath impact from less usage of PIN diodes and bi-directional properties has led to sustainable RF front-end system that is compact and require less energy usage as well as wideband operation properties. Therefore, this study proposes a new technique for wideband and high isolation of SPDT RF switches using switchable DGS in mm-wave telecommunications.

2. **Methods**

2.1. Mathematical Modeling of Switchable DGS

Theoretically, the bandstop response characteristics of a DGS have the potential to promote isolation. As depicted in Figure 2, it can be described as an LC equivalent circuit, where C_{DGS} and L_{DGS} represent the corresponding capacitance and inductance of the DGS, respectively [21]. The reason for using Simple LC modelling is used for the switchable DGS to gain fundamental knowledge of the DGS filter response (bandstop or allpass) when it is reconfigurable under the ideal switch condition. Mathematical modelling for this work does not introduce any novelty modelling as far as the research is concerned.

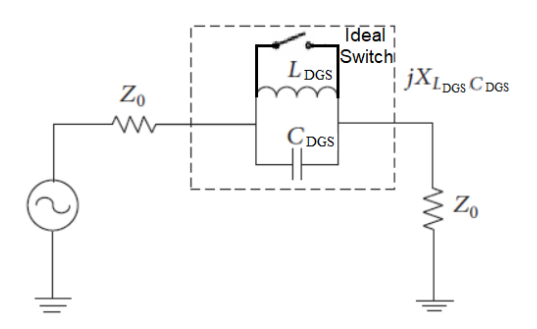


Figure 2. Equivalent circuit model of switchable DGS

Therefore, the impedance of DGS is given by Equation 1.

$$Z_{DGS} = jX_{LC} = \frac{\left(\frac{1}{j\omega C}\right)(j\omega L)}{\frac{1}{j\omega C} + j\omega L} = \frac{j\omega L}{1 - \omega^2 LC}$$
(1)

Then, the transfer matrix of the DGS in the ABCD parameters is given by Equation 2.

$$\begin{bmatrix} T_{DGS} \end{bmatrix} = \begin{bmatrix} 1 & Z_{DGS} \\ 0 & 1 \end{bmatrix} = \begin{bmatrix} 1 & \frac{j\omega L}{1 - \omega^2 LC} \\ 0 & 1 \end{bmatrix}$$
 (2)

Hence, from (2), using the conversion of ABCD to the S-parameter, the bandstop response of S_{21} is derived as in (3).

$$S_{21} = \frac{2}{A + \frac{B}{Z_0} + Z_0 C + D} = \frac{2}{2 + \frac{j\omega L}{\left(1 - \omega^2 L C\right) Z_0}}$$
(3)

where Z_0 is a characteristic impedance of the transmission line of the DGS.

Consider the PIN diode's off state, which should be an open circuit on the DGS. Consequently, the DGS acts as a bandstop. According to Equation 3, the L and C components are responsible for the notch of the bandstop if $Z_0 = I$, which is the normalized impedance. Prior to this, the DGS resonant frequency can be identified when the inductance reactance is equal to the capacitance reactance. As a result, the magnitude of bandstop notch S_{21} during the OFF state can be determined as Equation 4.

$$S_{21} = \frac{2}{2 + \infty} = 0 = \infty \ dB \tag{4}$$

From Equation 4, it can be observed that an ideally high attenuation can be achieved, where the notch of the bandstop response is produced. The following analysis considers an ON state in which the DGS should ideally be a short circuit. As a result, the DGS provides an allpass response. Theoretically, the allpass response can be generated if at least one or both the L and C components are zero. Considering that the ON state short-circuited the inductance of the DGS, L = 0 and letting $Z_0 = 1$, which is a normalized impedance, the S_{21} in the ON state is given by Equation 5.

$$S_{21} = \frac{2}{2+0} = 1 = 0 \, dB \tag{5}$$

From Equation 5, an ideal zero-insertion loss can be achieved, where the allpass response is produced. Based on mathematical analyses, further investigation into any EM simulation software such as CST Studio needs to be carried out for any type of DGS to make it switchable between bandstop and allpass responses. Different types of DGS have different effective capacitance and inductance that could be made switchable by one or more PIN diodes.

2.2. Mathematical Modeling of Discrete SPDT Switch with Switchable DGS

Figure 3 (a) shows the suggested circuit diagram for an SPDT series PIN diode with a switchable DGS. The PIN diodes are represented as D1 and D2. Figure 3 (b) depicts the equivalent circuit for the D1 and D2 PIN diodes, with R_f (forward resistance) and L_s (parasitic inductance from packaging) for the ON state and C_T (total capacitance from the diode junction and packaging) and R_p (reverse resistance) and L_s for the OFF state. In this study, PIN diodes with the model number MA4AGBLP912 from MACOM were used where R_f is 4 Ω , L_s is 0.5 pH, C_T is 26 fF and R_p is 10 k Ω which those values obtained from the SPICE model of the PIN diode parameters. Table 1 summarizes the parameters value.

As a result, Equation 6 and Equation 7 provide the transfer matrix of a series PIN diode in the ON and OFF states in the ABCD parameters.

$$\begin{bmatrix} T_{DI} \end{bmatrix} = \begin{bmatrix} 1 & R_f + j\omega L_s \\ 0 & 1 \end{bmatrix}$$
 (6)

$$[T_{D2}] = \begin{bmatrix} 1 & \frac{R_p + j\omega L_s - L_s C_T R_p \omega^2}{1 + j\omega C_T R_p} \\ 0 & 1 \end{bmatrix}$$
 (7)

Consider that the SPDT switch is in transmit mode, with DGS1 inactive and D1 in the ON state. Therefore, the transmit arm produces an allpass response that is connected to the insertion loss of port 2 from port 1 (S₂₁). DGS2 is active and D2 is in the OFF state while operating in the same mode. As a result, the isolation between ports 3 and 1 causes a bandstop response to be generated at the receiving arm (S₃₁). When D1 is in the OFF state and DGS1 is active, and when D2 is in the ON state and DGS2 is inactive, an identical operation (insertion loss to port 3 from port 2 and isolation between port 1 and port 2) may be obtained in the receive mode.

Given the state of the PIN diodes and DGSs in the SPDT switch during the transit mode, the transfer matrix of the circuit for insertion loss (S_{21}) and isolation (S_{31}) in the ABCD parameters is given by Equation 8 and Equation 9. Converting the transfer matrix in Equation 8 and Equation 9 into an Sparameter yields Equation 10 and Equation 11, respectively. Let Z_0 be a normalized impedance, and R_f and L_s be relatively small after normalization; thus, the insertion loss, S_{21} in Equation 10, is given by Equation 12, indicating an all-pass response. As the bandstop response of the DGS shows ideal infinite attenuation, the isolation, S_{31} in Equation 11, is given by Equation 13. According to Equation 13, additional isolation can be obtained by incorporating a switchable DGS into the SPDT switch design, which significantly improves the isolation performance when compared to the OFF state of a single PIN diode.

$$\begin{bmatrix} T_{IL} \end{bmatrix} = \begin{bmatrix} T_{DI} \end{bmatrix} \begin{bmatrix} T_{DGS} \end{bmatrix} \\
= \begin{bmatrix} 1 & \frac{j\omega L}{1 - \omega^2 L C} + R_f + j\omega L_s \\ 0 & 1 \end{bmatrix} \\
\begin{bmatrix} T_{Iso} \end{bmatrix} = \begin{bmatrix} T_{D2} \end{bmatrix} \begin{bmatrix} T_{DGS} \end{bmatrix}$$
(8)

$$= \begin{bmatrix} 1 & \frac{j\omega L}{1 - \omega^2 LC} + \frac{R_p + j\omega L_s - L_s C_T R_p \omega^2}{1 + j\omega C_T R_p} \\ 0 & 1 \end{bmatrix}$$
(9)

$$S_{21} = \frac{\frac{2}{j\omega L} - \frac{j\omega L}{1 - \omega^2 LC} + R_f + j\omega L_s}{2 + \frac{1 - \omega^2 LC}{Z_0}}$$
(10)

$$\begin{bmatrix}
T_{lso} \\ = T_{D2} \end{bmatrix} \begin{bmatrix} T_{DGS} \\ T_{DGS} \end{bmatrix} = \begin{bmatrix}
1 & \frac{j\omega L}{1 - \omega^2 LC} + \frac{R_p + j\omega L_s - L_s C_T R_p \omega^2}{1 + j\omega C_T R_p} \\ 0 & 1 \end{bmatrix}$$

$$S_{21} = \frac{2}{2 + \frac{j\omega L}{1 - \omega^2 LC} + R_f + j\omega L_s}$$

$$2 + \frac{2}{1 - \omega^2 LC} + \frac{R_p + j\omega L_s - L_s C_T R_p \omega^2}{1 + j\omega C_T R_p}$$

$$2 + \frac{2}{1 - \omega^2 LC} + \frac{R_p + j\omega L_s - L_s C_T R_p \omega^2}{1 + j\omega C_T R_p}$$

$$S_{21} = \frac{2}{2 + 0 + 0.08} = 1 = 0 dB$$

$$S_{31} = \frac{2}{2 + \omega + 4.73} = 0 = \omega dB$$

$$(12)$$

$$S_{21} = \frac{2}{2 + 0 + 0.08} = 1 = 0 \, dB \tag{12}$$

$$S_{31} = \frac{2}{2 + \omega + 4.73} = 0 = \omega dB \tag{13}$$

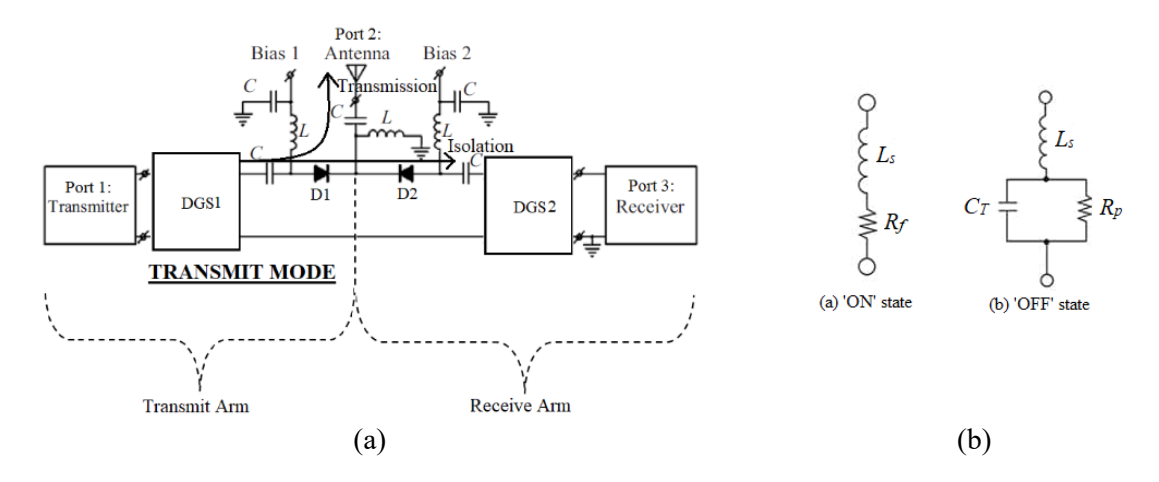


Figure 3. (a) SPDT series PIN diode with DGS and (b) PIN diode equivalent circuit model during (a) ON state and (b) OFF state

Table 1. MA4AGBLP912 PIN diode and Rogers RT/Duroid 5880 parameters value

Parameters	Value
$ m R_{f}$	$4~\Omega$
$L_{\rm s}$	0.5 pH
C_{T}	26 fF
R_p	10 kΩ
Thickness, h	0.254 mm
Copper Cladding Thickness, t	0.018 mm
Dielectric Constant, ε_r	2.2

2.3. Switchable DGS Design and Fabrication

The switchable DGS design is based on a conventional DGS, which controls its active and inactive conditions by switching elements, which are PIN diodes. Figure 4 (a) depicts a thin rectangular patch-switchable DGS based on [22]. A biasing circuit consisting of a biasing line and a radial stub was placed inside the DGS. Two PIN diodes were placed at the DGS with reference to the ground plane of the circuit, which can alter the reactance of the DGS and convert the response of the DGS from a bandstop to an allpass response. Hence, by applying a different bias voltage to the PIN diode, the circuit switches to an all-pass response. If no voltage (0 V) was applied to the biasing line, there would be no voltage difference between the diodes, causing them to be in the OFF state (open circuit). Hence, the DGS is active and functions as a bandstop filter. When a positive voltage (5 V) is applied to the biasing line, a voltage difference occurs in the diodes, resulting in an ON state (short circuit). Hence, the DGS was inactive and acted as an all-pass filter. Radial stubs act as RF chokes that prevent any RF signal from interfering with the biasing supply of PIN diodes. Figure 4 (b) and Figure 4 (c) show the top and bottom views of the circuit layout respectively using the DGS in the microstrip line model. The switchable DGS design was simulated using CST Microwave Studio software, and the performance was analyzed in terms of attenuation, insertion loss, and return loss.

Figure 5 (a) and Figure 5 (b) show top and bottom views of the fabricated switchable DGS respectively. The Rogers RT/Duroid 5880 substrate, which has a thickness of 0.254 mm and a relative dielectric constant $\varepsilon_r = 2.2$, was used to construct the switchable DGS. Table 1 summarizes the parameters value. To guarantee that conductivity was formed between the PIN diodes and the desired circuit structures, PIN diodes were placed using conductive glue that was cured at room temperature for 24 hours. Figure 5 (c) shows the measurement setup for the manufactured switchable thin rectangular patch DGS. To measure the isolation, insertion loss, and return loss of the prototype, a network analyzer

was used in combination with several RF components, such as high-precision coaxial cables, DC blocks, and connectors. The prototype's isolation, insertion loss, and return loss were then verified using the simulation results from CST Microwave Studio and mathematical models.

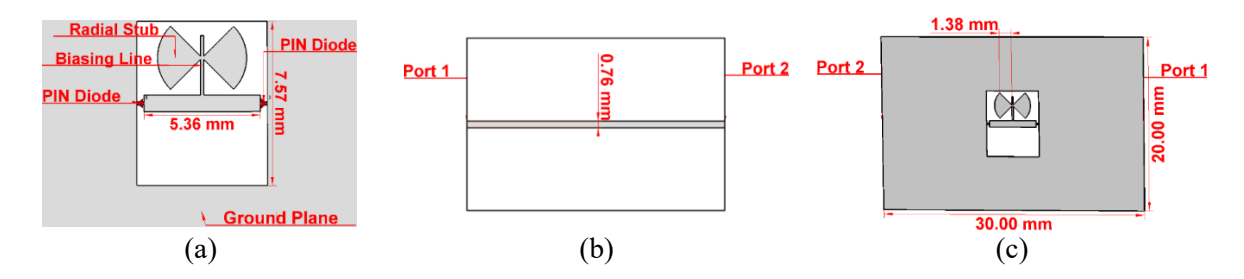


Figure 4. (a) Circuit layout for switchable DGS, (b) top view of switchable DGS full circuit and (c) bottom view of switchable DGS full circuit

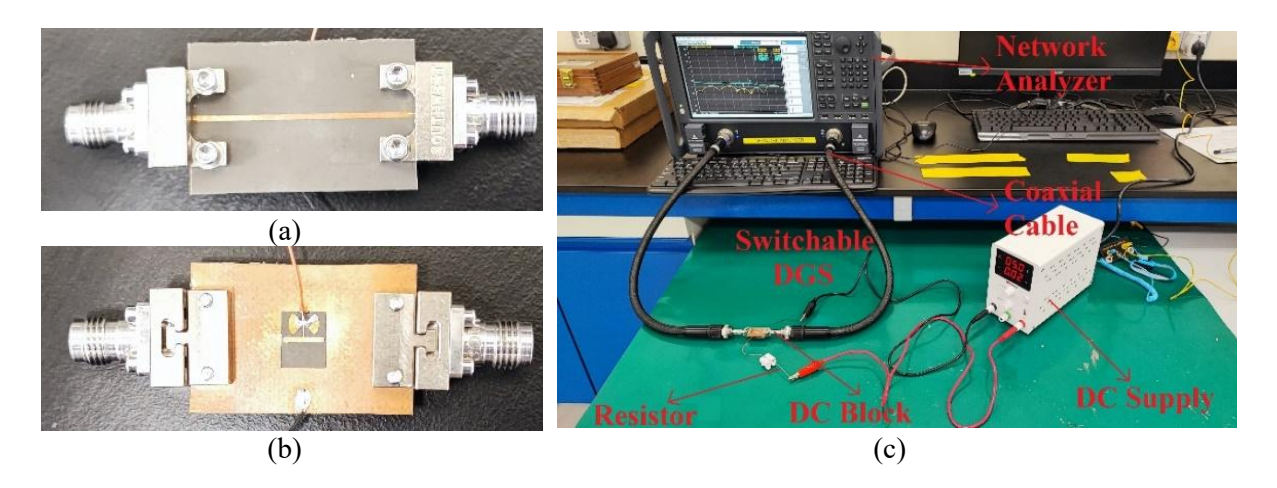


Figure 5. (a) Top view of fabricated switchable DGS, (b) bottom view of fabricated switchable DGS and (c) measurement setup for the fabricated switchable DGS

2.4. SPDT Switch with the Switchable DGS Design and Fabrication

The distinguish difference between the proposed SPDT switch design with other related works such as [11], [12], [23], [24] are the design is implemented in mm-wave region with the usage of solid-state PIN diodes on discrete setup which is much different from the heavily used lower frequency spectrum and Microelectromechanical Systems (MEMS) or Complementary Metal Oxide Semiconductor (CMOS) switches that is monolithic integrated setup. Figure 6 (a) and Figure 6 (b) depict the top and bottom views of the discrete SPDT switch design respectively with a thin rectangular patch DGS. As the SPDT switch design is symmetrical between both the transmit and receive arms, the explanation in this section focuses on the transmit mode operation because it reflects the same result as the receive mode operation. However, the summary for both operating conditions is tabulated later for easier reference. Hence, during the transmission mode, 5 V was applied to the V1 and V3 bias lines, resulting in the D1 PIN diode turning ON. A voltage of 5 V was also applied to the D3 and D4 PIN diodes on the DGS1. This results in a short-circuit path from port 1 to port 2, where RF signal transmission occurs and deactivates the DGS1 functionality. Consequently, the transmit arm functions as an all-pass filter. At the same time, 0 V was applied to the V2 and V4 bias lines, resulting in the D2 PIN diode turning OFF. A voltage of 0 V was applied to the D5 and D6 PIN diodes on the DGS2. This results in an open circuit path from port 1 and port 2 to port 3, as well as enhanced isolation of the RF signal with the activation of DGS2. Consequently, the receiver arm functions as a bandstop filter. As a whole, the RF signal can transmit

from the transmitter to the antenna because of the allpass response at the transmit arm, and any leakage signal from both the transmitter and antenna is isolated by the bandstop response at the receive arm.

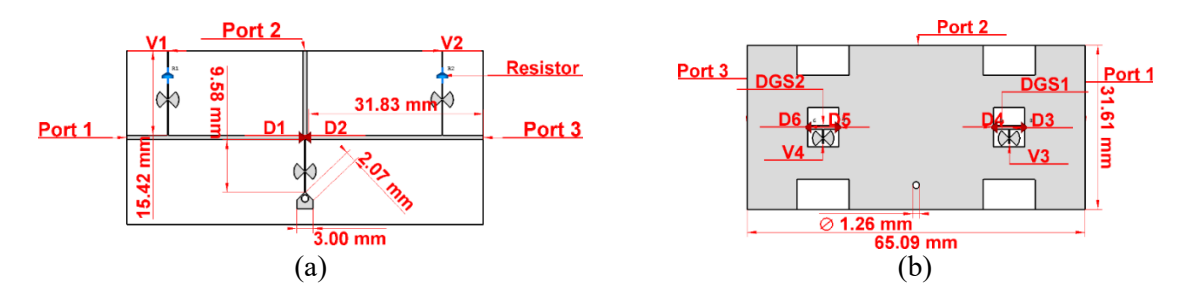


Figure 6. Circuit layout of SPDT switch with switchable DGS from (a) top view and (b) bottom view

As previously described, the SPDT switch with a switchable DGS was simulated in CST Microwave Studio software, and the performance was analyzed in terms of isolation, insertion loss, and return loss. Figure 7 (a) and Figure 7 (b) shows the top and bottom views of the fabricated SPDT switch respectively with a switchable DGS using a Rogers RT/Duroid 5880 substrate. Meanwhile, Figure 7 (c) and Figure 7 (d) shows the measurement setup for the fabricated SPDT switch with a switchable thin rectangular patch DGS. Compared to the measurement setup of the switchable DGS, there is an addition of a 50 Ω termination, which is used to ensure that the RF signal propagates to port 3 in the receive arm by matching the port to a microstrip line on the circuit.

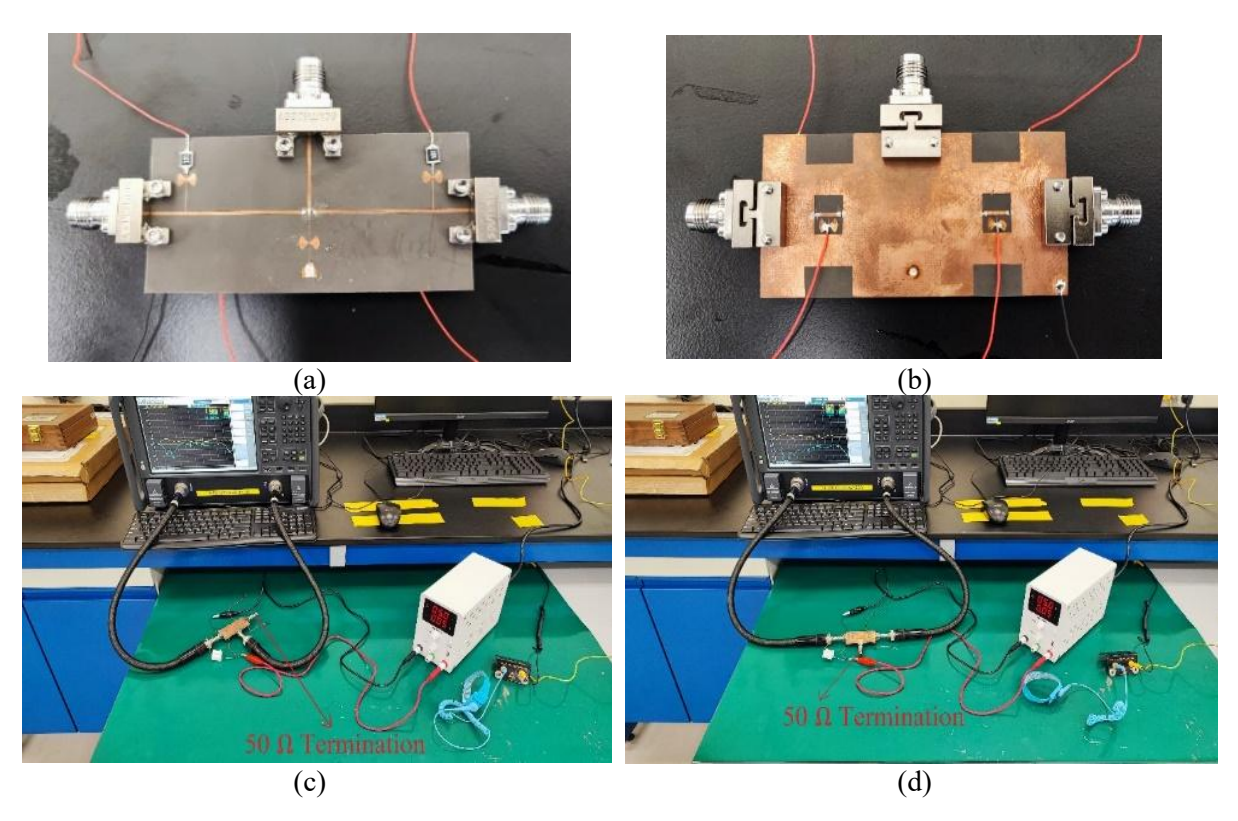


Figure 7. (a) Top view of the fabricated SPDT switch with the switchable DGS, (b) bottom view of the fabricated SPDT switch with the switchable DGS, (c) return loss/ insertion loss measurement setup for the fabricated SPDT switch with the switchable DGS and (d) isolation measurement setup for the fabricated SPDT switch with the switchable DGS

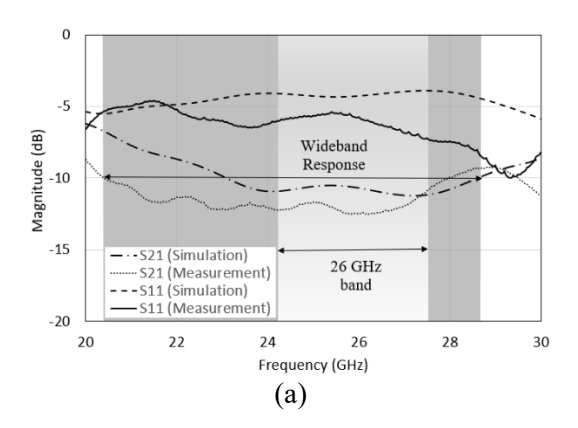
3. Results and Discussion

3.1. Thin Rectangular Patch Switchable DGS Performance

Ahead of the results discussion, it is important to mention that network analyzer used is the N5234B PNA-L Microwave Network Analyzer from Keysight. It can measure from a frequency range of 10 MHz to 43.5 GHz. During calibration process, which is prior before commencing any measurements, the measurement uncertainty obtained is around ± 0.98 dB for range of frequency from 20 to 43.5 GHz. Since the uncertainty absolute value is less than 1 dB, it can be determined that the measurement results produced are accurate and precise.

The results of the thin rectangular patch switchable DGS when the DGS is active are shown in Figure 8 (a) for both the simulated and measured results. As is evident, the active DGS has demonstrated bandstop properties with an attenuation level (S₂₁) larger than 10 dB, a fractional bandwidth (FBW) of 21.7% spanning from 23.05 to 28.66 GHz for simulation, and an FBW of 31.37% ranging from 20.41 to 28 GHz for measurement. Owing to the interconnections of the inductance of the discrete components, the measured bandwidth is significantly larger than the simulated value [25]. The bonding process between the PIN diodes and the circuit structure is claimed to have decreased the Q factors of the matching networks, which led to an enhanced bandwidth. However, both results demonstrate that the active switchable DGS has a wideband bandstop response and is thus appropriate for the wideband isolation performance of an RF SPDT switch. Furthermore, the frequency range also covers the 26 GHz mm-wave band with a stopband return loss (S₁₁) of less than 10 dB, which indicates that less signal is transmitted and mimics the function of isolation in an RF switch. Meanwhile, the attenuation analysis in Equation 4 is said to be related to the simulation and measurement results in Figure 12, as both results show that good attenuation (more than 10 dB) was achieved.

Figure 8 (b) shows the simulated and measured results of the thin rectangular patch-switchable DGS when the DGS is deactivated. The inactive DGS has all-pass properties, with an insertion loss (S₂₁) of less than 1.5 dB in the 26 GHz simulation band and less than 5 dB in the same band for measurement. Distributed capacitance and inductance effects from the bonding of discrete components [16], [26] and conductor loss due to a thin substrate [27] have been identified as causing higher insertion loss in measurement results compared to simulation. Despite the uncertainty, both results are quite satisfactory and hence show that the inactive switchable DGS produces an allpass response for RF signal transmission during the closed-switch condition. Furthermore, the passband return loss, or return loss (S₁₁), is greater than 10 dB, indicating that fewer RF signals are reflected. This proves that most RF signals are transmitted from the input port during the closed switch condition. Meanwhile, the insertion loss analysis in Equation 5 is said to be related to the simulation and measurement results in Figure 8 (b), as both results showed that a good insertion loss (less than 5 dB) was achieved.



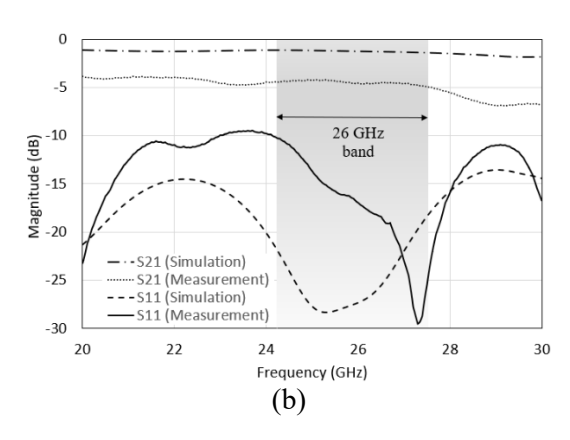


Figure 8. (a) Simulated and measured results of attenuation (S_{21}) and stopband return loss (S_{11}) of the active switchable DGS and (b) simulated and measured results of insertion loss (S_{21}) and return loss (S_{11}) of the inactive switchable DGS

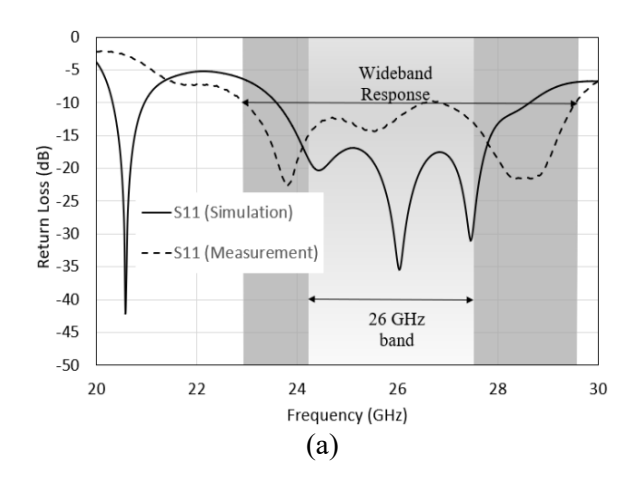
3.2. SPDT Switch with the Switchable DGS Performance

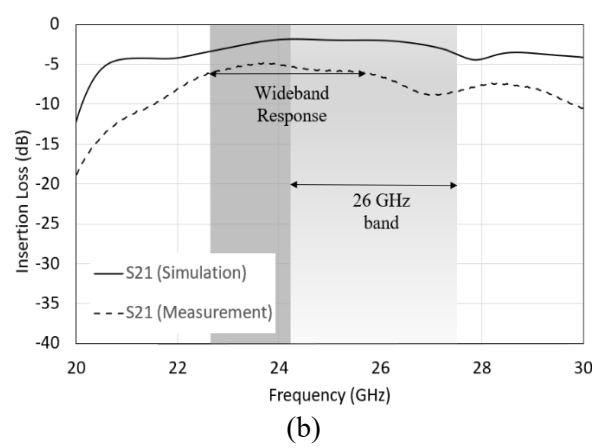
Figure 9 shows the simulated and measured results of the switchable DGS SPDT during the transmission mode, where the transmit arm side is in the ON state and the receive arm side is in the OFF state. The same output was obtained in receive mode. The results are as follows: return loss (S_{11}) in Figure 9 (a), insertion loss (S_{21}) in Figure 9 (b), and isolation loss (S_{31}) in Figure 9 (c).

Figure 9 (a) shows that the return loss (S_{11}) is more than 10 dB with an FBW of 25.29%, ranging from 22.94 to 29.58 GHz for measurement, which is far larger than the simulation with an FBW of 19.41% ranging from 23.58 to 28.65 GHz. Because the switchable DGS is also a part of the SPDT switch, the same effect of wider bandwidth occurred at the 10 dB level owing to a decrease in the Q factor from parasitic inductance at the conductive connections of diodes D3 and D4 on the DGS structure as well as D1 diode on the microstrip line. Despite this difference, the return loss results of the switchable DGS SPDT switch indicate that less RF signal is reflected in Port 1, thus increasing the chances for most of the RF signals to be channeled to Port 2, where the antenna is placed in the real application. However, the RF signal factor successfully transmitted to Port 2 was also determined by the insertion loss (S_{21}) of the switchable DGS SPDT switch.

As depicted in Figure 9 (b), the insertion loss (S₂₁) is less than 6 dB with FBW of 37.81% ranging from 20.46 to 30 GHz for simulation and FBW of 12.73% ranging from 22.66 to 25.74 GHz for measurement. The S₂₁ bandwidth of the measured SPDT switch has shown some reduction which can be related to the addition of series PIN diodes D1, D3 and D4 that adds more stray capacitance and inductance as well as additional resistance effects through its bonding. This addition also has significantly shifted insertion loss to lower frequency range. On top of that, since mm-wave circuits have propagation of smaller wavelength, thinner substrate is needed to minimize spurious signal generation that can produce unwanted resonance [28]. However, the thin substrate led to higher conductor loss during high frequency operation and thus contributed to insertion loss. Therefore, this trade-off somehow must be balanced to produce optimum results of the insertion loss. Meanwhile, the insertion loss analysis in Equation 12 is found to be like the simulated and measurement results in Figure 9 (b) as both results showed that good insertion loss (less than 6 dB) are achieved.

The isolation (S₃₁) in Figure 9 (c) is more than 25 dB with both simulation and measurement obtained the FBW of 25.24% ranging from 20 to 25.78 GHz. Based on the high isolation obtained, the switchable DGS on the SPDT switch circuit had the ability to isolate the receive arm part from possible power leakage during transmission process from Port 1 to Port 2. Meanwhile, the isolation analysis in Equation 13 tallies with the simulated and measurement results in Figure 9 (c) as both results showed that high isolation (more than 25 dB) are achieved. Therefore, the proposed SPDT switch with switchable DGS can be implemented in any mm-wave communication system such as Industry on Internet of Things (IIoT) as mentioned in [29].





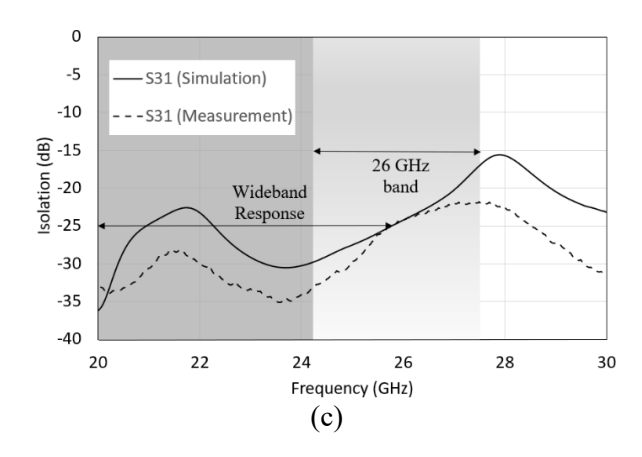


Figure 9. Simulated and measured results of (a) return loss (S_{11}) , (b) attenuation (S_{21}) and (c) isolation (S_{31}) of the thin rectangular patch switchable DGS SPDT switch

Figure 10 shows a measurement comparison between the switchable DGS SPDT switch and conventional SPDT switch (without DGS). The isolation (S₃₁) results further prove that the switchable DGS is a distinct factor for improving the isolation magnitude of the SPDT switch. The switchable DGS SPDT switch has improved isolation by approximately 10 dB to 15 dB in the 26 GHz band compared to the conventional SPDT. There were no distinct changes in the return loss (S₁₁) and insertion loss (S₂₁) for either simulated circuit, as both parameters were from the allpass response in which the DGS was inactive. Finally, Table 2 summarizes the measurement comparison of SPDT performances for both switchable DGS SPDT switch and conventional SPDT switch. This analysis is important to identify the better performance of switchable DGS SPDT switch compared to conventional SPDT switch at operational frequency in the 26 GHz band.

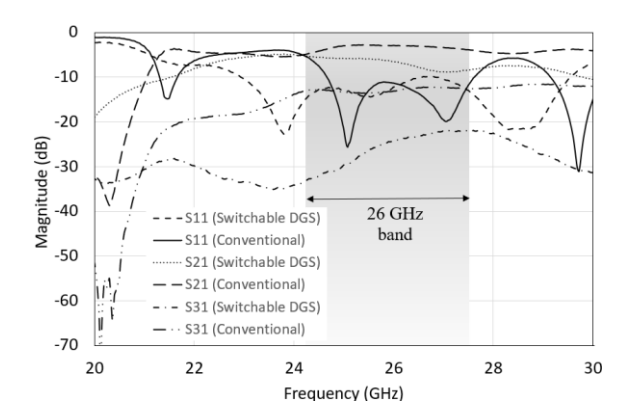


Figure 10. Measurement comparison between the switchable DGS SPDT switch and conventional SPDT switch (without DGS)

Table 2. Measurement comparison between switchable DGS SPDT switch and conventional switch

Performance Parameter	SPDT Switch Design	Simulation Magnitude at 25.875 GHz (dB)	Measurement Magnitude at 25.875 GHz (dB)
Return Loss (S ₁₁)	Conventional	16.35	11.15
	Switchable DGS	27.67	13.13
Insertion Loss (S ₂₁)	Conventional	1.63	2.93
	Switchable DGS	1.99	6.30
Isolation (S ₃₁)	Conventional	11.27	13.25
	Switchable DGS	24.64	24.58

4. Conclusion

A thin rectangular patch-switchable DGS SPDT switch was successfully designed for mm-wave telecommunication applications. A switchable DGS can be configured between the bandstop and allpass responses. The simulated results using CST Microwave Studio software and the measured results showed good agreement between the return loss (S_{11}) and isolation (S_{31}) results, which were greater than 10 dB and more than 25 dB, respectively. However, there is some offset in the insertion loss (S21) measurement results in terms of the degradation magnitude and frequency shifting towards the lower range owing to bonding parasitic effects. In general, the thin rectangular patch switchable DGS has the potential to be used in SPDT switches because it contributes to the wideband and high isolation of the switch. Therefore, the use of a switchable DGS has introduced a new technique to obtain wideband and high isolation for the SPDT RF switch. For future recommendations, this proposed work is suitable to be implemented as system-on-chip (SoC) as the high wideband isolation obtained, made capable for the integration of the RF transmitter and receiver on the same substrate, as well as the antenna and the SPDT switch. Furthermore, implementation of machine learning and genetic algorithms as mentioned in [30] and [31] can reduce the design time as well as improve modeling accuracy. Considering its implementation can aid in designing more complex SPDT switches to obtain wideband isolation response in less iteration time.

Acknowledgements

The authors would like to greatly express their thanks and appreciation to the Centre for Research and Innovation Management (CRIM) and Universiti Teknikal Malaysia Melaka (UTeM) for their help in completing this research work.

References

- [1] N. A. Shairi, A. M. Zobilah, Z. Zakaria, A. Othman, and S. Y. Weng, "Design and analysis of a dual function of switchable resonator for RF switch," in *Journal of Physics: Conference Series*, 2020, pp. 1–8. doi: 10.1088/1742-6596/1502/1/012026
- [2] International Telecommunication Union, "Setting the scene for 5G: Opportunities & Challenges," 2018.
- [3] B. Yang, Z. Yu, J. Lan, R. Zhang, J. Zhou, and W. Hong, "Digital beamforming-based massive MIMO transceiver for 5G millimeter-wave communications," *IEEE Trans Microw Theory Tech*, vol. 66, no. 7, pp. 3403–3418, 2018, doi: 10.1109/TMTT.2018.2829702.
- [4] A. Semnani, S. O. Macheret, and D. Peroulis, "A quasi-absorptive microwave resonant plasma switch for high-power applications," *IEEE Trans Microw Theory Tech*, vol. 66, no. 8, pp. 3798–3806, 2018, doi: 10.1109/TMTT.2018.2834925.
- [5] N. A. Tarek, R. Hokayem, S. R. Govindarajulu, M. H. Novak, and E. A. Alwan, "A Two-Stage Wideband RF Cancellation of Coupled Transmit Signal for Bi-Static," *IEEE Journal of Microwaves*, vol. 2, no. 3, pp. 429–441, 2022, doi: 10.1109/JMW.2022.3177578.

- [6] A. Kumar and A. P. Singh, "Enhancement of the Performance Parameters of Microstrip Slotted Patch Antenna using Defected Ground Structure," *International Journal of Engineering Trends and Technology*, vol. 60, no. 2, pp. 122–127, 2019, doi: 10.14445/22315381/IJETT-V60P217.
- [7] R. Kumar Nirala, "An overview on defected ground structure in aspect of microstrip patch antenna," *International Journal on Recent and Innovation Trends in Computing and Communication*, vol. 6, no. 1, pp. 31–34, 2018, [Online]. Available: http://www.ijritcc.org
- [8] E. G. Ouf, E. A. F. Abdallah, A. S. Mohra, and H. M. S. Elhennawy, "Electronically switchable ultra-wide band/dual-band bandpass filter using defected ground structures," *Progress In Electromagnetics Research C*, vol. 91, pp. 83–96, 2019, doi: 10.2528/pierc19010702.
- [9] A. H. Jabire, A. Abdu, S. Saminu, A. M. Sadiq, and M. J. Adamu, "Isolation Frequency Switchable MIMO Antenna for PCS, WIMAX and WLAN Application," *ELEKTRIKA-Journal of Electrical Engineering*, vol. 18, no. 3, pp. 27–33, 2019, doi: 10.11113/elektrika.v18n3.178.
- [10] S. Riaz, X. Zhao, and S. Geng, "A frequency reconfigurable MIMO antenna with agile feedline for cognitive radio applications," *International Journal of RF and Microwave Computer-Aided Engineering*, vol. 30, no. 3, pp. 1–9, 2020, doi: 10.1002/mmce.22100.
- [11] K. Han, Y. Liu, X. Guo, Z. Jiang, N. Ye, and P. Wang, "Design, analysis and fabrication of the CPW resonator loaded by DGS and MEMS capacitors," *Journal of Micromechanics and Microengineering*, vol. 31, no. 6, 2021, doi: 10.1088/1361-6439/abf844.
- [12] A. A. Ibrahim, H. A. Mohamed, A. R. D. Rizo, R. Parra-Michel, and H. Aboushady, "Tunable Filtenna With DGS Loaded Resonators for a Cognitive Radio System Based on an SDR Transceiver," *IEEE Access*, vol. 10, pp. 32123–32131, 2022, doi: 10.1109/ACCESS.2022.3160467.
- [13] A. M. Zobilah, Z. Zakaria, and N. A. Shairi, "Selectable multiband isolation of single pole double throw switch using transmission line stub resonator for WiMAX and LTE applications," *IET Microwaves, Antennas and Propagation*, vol. 11, no. 6, pp. 844–851, 2017, doi: 10.1049/ietmap.2016.0868.
- [14] N. A. Shairi, A. M. Zobilah, B. H. Ahmad, and Z. Zakaria, "Design comparison of RF SPDT switch with switchable resonators for wiMAX and LTE in 3.5 GHz band," *International Journal of Applied Engineering Research*, vol. 12, no. 20, pp. 9614–9618, 2017.
- [15] L. Zhang, X. Cheng, X. Deng, and X. Li, "Design of K/KA-band Passive HEMT SPDT Switches with High Isolation," in 2017 China Semiconductor Technology Internation Conference (CSTIC), 2017, pp. 3–6.
- [16] Y. Gong, J. W. Teng, and J. D. Cressler, "A Compact, High-Power, 60 GHz SPDT Switch Using Shunt-Series SiGe PIN Diodes," in *Digest of Papers IEEE Radio Frequency Integrated Circuits Symposium*, 2019, pp. 15–18. doi: 10.1109/RFIC.2019.8701812.
- [17] S. Jang, S. Kong, H. D. Lee, J. Park, K. S. Kim, and K. C. Lee, "28 GHz 1.8 dB Insertion Loss SPDT Switch with 24 dB Isolation in 65 nm CMOS," in 2018 48th European Microwave Conference, EuMC 2018, 2018, pp. 835–838. doi: 10.23919/EuMC.2018.8541696.
- [18] N. A. Shairi, Y. A. G. Mohammed, Z. Zakaria, M. A. M. Said, M. H. Misran, and Z. Z. A. Mohammed, "Performance Comparison of UWB Single Balanced Schottky Diode Mixers for RF Front-End Applications in 3-10 GHz Band," *Advance Sustainable Science, Engineering and Technology*, vol. 7, no. 2, Feb. 2025, doi: 10.26877/asset.v7i2.1579.
- [19] J. Zhang *et al.*, "An Ultra-Compact Bidirectional Ka-Band Front-End Module With 3.8-dB NF and 13.5-dBm OP1 dB," *IEEE Microwave and Wireless Technology Letters*, vol. 33, no. 1, pp. 70–73, Jan. 2023, doi: 10.1109/LMWC.2022.3202899.
- [20] S. Kim, J. Jeong, B.-W. Min, and J. Han, "28-GHz Bidirectional RF CMOS Amplifier Employing Body-Effect Control," *IEEE Microwave and Wireless Technology Letters*, vol. 33, no. 6, pp. 695–698, Feb. 2023, doi: 10.1109/lmwt.2023.3241603.
- [21] M. K. Khandelwal, B. K. Kanaujia, and S. Kumar, "Defected ground structure: fundamentals, analysis, and applications in modern wireless trends," *Int J Antennas Propag*, vol. 2017, 2017, doi: 10.1155/2017/2018527.

- [22] B. H. Ahmad, N. A. Shairi, and J. Saveridass, "Low Cost Tunable Bandstop Filter Design of Defected Ground Structure using FR4 Substrate," *International Journal of Electronics and Computer Science Engineering*, vol. 2, no. 2, pp. 595–601, 2013.
- [23] H. B. El-Shaarawy, F. Coccetti, R. Plana, M. El-Said, and E. A. Hashish, "Novel reconfigurable defected ground structure resonator on coplanar waveguide," *IEEE Trans Antennas Propag*, vol. 58, no. 11, pp. 3622–3628, 2010, doi: 10.1109/TAP.2010.2071336.
- [24] T. Kim, H. D. Lee, B. Park, S. Jang, S. Kong, and C. Park, "Design of a K-Band High-Linearity Asymmetric SPDT CMOS Switch Using a Stacked Transistor," *IEEE Microwave and Wireless Components Letters*, vol. 32, no. 12, pp. 1443–1446, Dec. 2022, doi: 10.1109/LMWC.2022.3192440.
- [25] P. Song, R. L. Schmid, A. Ç. Ulusoy, and J. D. Cressler, "A high-power, low-loss W-band SPDT switch using SiGe PIN diodes," in *Digest of Papers IEEE Radio Frequency Integrated Circuits Symposium*, 2014, pp. 195–198. doi: 10.1109/RFIC.2014.6851695.
- [26] K. Lam *et al.*, "Wideband millimeter wave PIN diode SPDT switch using IBM 0.13μm SiGe technology," in *Proceedings 2nd European Microwave Integrated Circuits Conference, EuMIC 2007*, 2007, pp. 108–111. doi: 10.1109/EMICC.2007.4412659.
- [27] J. Coonrod, "Insertion loss comparisons of common high frequency PCB constructions," in *IPC APEX EXPO Conference and Exhibition 2013, APEX EXPO 2013*, 2013, pp. 870–884.
- [28] J. Coonrod, "The effect of radiation losses on high frequency PCB performance," in *IPC APEX EXPO Conference and Exhibition 2014, APEX EXPO 2014*, 2014, pp. 1–9.
- [29] R. P. Astutik, J. Lesmana Putra, and R. Maulana, "Design of IIOT Device Based on LoRa for Parsing Data Directly to SCADA System," *Advance Sustainable Science, Engineering and Technology*, vol. 6, no. 3, May 2024, doi: 10.26877/asset.v6i3.813.
- [30] Abdillah, Syaharuddin, V. Mandailina, and S. Mehmood, "The Role of Mathematics in Machine Learning for Disease Prediction: An In-Depth Review in the Healthcare Domain," *Advance Sustainable Science, Engineering and Technology*, vol. 6, no. 4, Aug. 2024, doi: 10.26877/asset.v6i4.845.
- [31] A. N. A. Yusuf, P. D. Purnamasari, and F. Y. Zulkifli, "Optimization of Defected Ground Structure (DGS) Using Genetic Algorithm for Gain Enhancement of Microstrip Antenna," in 2021 IEEE Asia-Pacific Conference on Applied Electromagnetics, 2021, pp. 2021–2024.